Earth and Planetary Science Letters 579 (2022) 117371

Contents lists available at ScienceDirect

Earth and Planetary Science Letters

www.elsevier.com/locate/epsl

Local melt contamination and global climate impact: Dating the emplacement of Karoo LIP sills into organic-rich shale

Sean P. Gaynor [a,*], Henrik H. Svensen [b], Stéphane Polteau [c], Urs Schaltegger [a]

[a] Department of Earth Sciences, University of Geneva, 1205, Geneva, Switzerland
[b] Centre for Earth Evolution and Dynamics (CEED), University of Oslo, P.O. Box 1028 Blindern, 0315 Oslo, Norway
[c] Institute for Energy Technology (IFE), P.O. Box 40, 2027, Kieller, Norway

ARTICLE INFO

Article history:
Received 16 September 2021
Received in revised form 31 December 2021
Accepted 9 January 2022
Available online 17 January 2022
Editor: C.M. Petrone

Keywords:
Karoo
Large Igneous Provinces
isotope geochronology
Toarcian Oceanic Anoxic Event

ABSTRACT

The emplacement of Large Igneous Provinces (LIPs) is commonly correlated with global climate change, and environmental and biological crises. To establish this complex causative link, chemical proxies from marine sedimentary sections must be temporally tied to LIP activity through high-precision geochronology. The temporal link is often ambiguous, especially as periods of environmental change are commonly shorter than the full duration of magmatic and volcanic activity in a LIP. Most importantly, temporal relations need to be established through precise and accurate U-Pb geochronology; however, mafic rocks are often undersaturated in zircon or baddeleyite. New U-Pb age determinations of pegmatitic pods from Karoo LIP dolerite sills into the Ecca Group of the Karoo Basin yield single crystal dates with uncertainties below 50 ka, which allow for a new, detailed assessment of this intrusive event. These samples yield complicated age spectra and Hf geochemistry, which indicate that localized assimilation of sedimentary rocks enabled zircon saturation within these mafic melts. Zircon crystallization age interpretations from these data indicate that sill emplacement within the Ecca Group was coeval across the basin within uncertainty of U-Pb dating, and therefore represents a period of particularly high magma flux. Since the Ecca Group is locally exceptionally rich in organic matter, the widespread and rapid sill-related contact metamorphism generated a significant volume of thermogenic volatiles. Given the temporal overlap of the emplacement of sills between 183.147 ± 0.059 Ma and 183.187 ± 0.133 Ma and the timing of the global Toarcian Oceanic Anoxic Event (TOAE), our data support a causal link between this discrete period of high flux emplacement of Karoo sills into the Ecca Group and the global climate change that took place during the Early Jurassic.

1. Introduction

Large igneous provinces (LIPs) are composed of massive volumes of lava flows and extensive plumbing systems including sills and dikes, commonly driven by deep mantle processes (e.g., Bryan and Ernst, 2008). Many of these voluminous events in Earth's history have also been commonly associated with extinction events and perturbations in global climate (e.g., Bond and Wignall, 2014), leading to an abundance of research investigating these ties through geologic time. The degassing of these voluminous magmas during ascent and crystallization can contribute an abundance of mantle-derived volatiles to the atmosphere (e.g., CO_2, SO_2, HCl, HF; Capriolo et al., 2020). Volatile release can induce global warming depending on the fluxes, volumes and atmospheric residence times of these gases, and subsequent weathering of basalt results in long term cooling due to CO_2 fixation into alteration minerals (e.g., Self et al., 2014). Workers have recognized that the release of "thermogenic" CH_4, CO_2, SO_2 and CH_3Cl from contact metamorphosed carbon-rich or evaporitic sedimentary rocks is an important process to explain global climate change contemporaneous to LIP magmatism (e.g., Svensen et al., 2007; Aarnes et al., 2010). Thus, the injection of large volumes of both magmatic and thermogenic isotopically light carbon can explain the observed negative carbon isotope excursions, which provide the causal link between LIPs and global climatic and environmental change.

Recent high-precision geochronology studies have suggested at least partial decoupling of LIP activity and periods of extreme carbon cycle variations (e.g., De Lena et al., 2019), while the synchronicity of LIPs and environmental perturbations have been confirmed in other examples (e.g., Burgess et al., 2015; Schoene et al., 2019; Kasbohm et al., 2021). In addition, LIPs are incredibly large in scale, commonly over 1 Mkm^3, and therefore the development

* Corresponding author.
E-mail address: sean.gaynor@unige.ch (S.P. Gaynor).

https://doi.org/10.1016/j.epsl.2022.117371

of robust, high-precision geochronology datasets are necessary to truly characterize these relationships. The durations of climate perturbations and related extinction events are far shorter than the observed lifespan of individual LIPs, and as result any connection between the two is likely due to discrete periods of high magma flux during LIP emplacement (e.g., Burgess et al., 2017; Schoene et al., 2019). Therefore, new and precise geochronology data are required to better explore the potential causality of LIPs for environmental change.

The intrusive component of the Karoo LIP, in large part emplaced in Late Carboniferous to Early Jurassic sedimentary strata of the Karoo Basin in South Africa, serves as an excellent case study to investigate the connections between LIPs and climate change, as the subvolcanic domain is well-exposed and drilled. Previous geochronology has indicated this magmatic activity as coeval with the presumably global Toarcian Oceanic Anoxic Event (TOAE; e.g., Svensen et al., 2012; Sell et al., 2014; Burgess et al., 2015; Corfu et al., 2016; Greber et al., 2020). Recent advances in U-Pb geochronology allow a temporal resolution ($\pm 2\sigma$) of as low as 50,000 years for individual zircon in this age range. Therefore, our ability to temporally correlate the release of thermogenic volatiles into the atmosphere during sill emplacement with marine anoxia has improved significantly. The Ecca Group contains organic-rich sedimentary rocks across the basin and is suggested to represent the main carbon source behind the Toarcian carbon cycle perturbations (Svensen et al., 2007). Contact metamorphism and subsequent degassing through hundreds of pipe structures may have released more than 7,000 Gt CO_2 to the atmosphere, with an upper range of above 50,000 Gt (e.g., Svensen et al., 2007; Aarnes et al., 2010; Galerne and Hasenclever, 2019; Svensen et al., 2020). While existing geochronology from the Karoo Basin has already shown concurrence between the LIP emplacement and the Early Jurassic climate change, more high-precision geochronology is needed to gain a better understanding of the timing and the tempo of sill emplacement and subsequent contact metamorphic volatile release.

We dated dolerite sills emplaced in the Ecca Group of the Karoo Basin, and present geochemical and textural data of zircon and baddeleyite to test for a causal relationship with the TOAE. Our new data show that the crystallization of zircon within mafic LIP sills can be far more complicated than simple fractionation of a silicic melt from differentiation of mafic melts, but instead records a history of incorporating sedimentary host rocks through melting and pore fluids into crystallizing magma. The incorporation of xenocrystic zircon at the emplacement level, combined with unmitigated Pb-loss due to elevated U concentrations, generates complicated U-Pb age spectra; however, these spectra can yield age plateaus representative of crystallization age. We interpret these ages to reflect coeval emplacement of mafic sills throughout the Ecca Group within analytical uncertainty, indicating they caused a rapid injection of massive volumes of basin-derived carbon into the atmosphere. Given that these ages are all within uncertainty of the TOAE, we support that the devolatilization of shales in the Ecca Group may have been causative for global climate perturbations within the Toarcian.

2. Geological setting

The Karoo LIP includes extrusive and intrusive rocks spread across southern Africa and western Antarctica (e.g., Duncan et al., 1997), with the main volume focused on the Karoo basin and emplaced during a brief time interval in the Jurassic (e.g., Svensen et al., 2012; Greber et al., 2020). The intrusive component is characterized by an extensive sill and dike network within the clastic sedimentary rocks of the Karoo Basin, covered by the Drakensberg Group flood basalts. While the Dwyka, Beaufort and Stormberg groups are composed predominantly of siltstones and sandstones, the Ecca Group is the only portion of the Karoo Basin with abundant organic-rich shales (Fig. 1). The LIP sills currently comprise approximately 30% of the Karoo Basin's thickness, exposed as saucer-shaped (e.g., the Golden Valley sill), nested intrusions in the upper part of the stratigraphy (Fig. 1; e.g., Neumann et al., 2011; Svensen et al., 2014). The sills in the Ecca Group are predominantly extensive (>200 km) planar sheets, emplaced concordantly within the sedimentary host rocks, and are the thickest sills in the basin. These sills represent 160,000 km^3 of the estimated 340,000 km^3 of intrusions emplaced within the basin (Svensen et al., 2012).

While many early studies of Karoo geochronology utilized Ar-Ar techniques (e.g., Duncan et al., 1997; Jourdan et al., 2008), recent efforts on understanding the timing of the Karoo Basin intrusions have focused on U-Pb dating of zircon, either separated from coarse-grained intrusions found in the upper stratigraphy, or from pegmatitic pods within fine-grained intrusions (Svensen et al., 2012; Sell et al., 2014; Burgess et al., 2015; Greber et al., 2020). An exhaustive zircon U-Pb study from pegmatites indicated that the sills were emplaced from 183.0 ± 0.5 to 182.3 ± 0.6 Ma, with little temporal dispersion within individual samples (Svensen et al., 2012).

The emplacement of dolerite sills in the Karoo Basin caused widespread volatile release from contact metamorphism and pore fluid heating, leading to phreatic and phreatomagmatic activity (Svensen et al., 2006, 2007). Within the Ecca Group, the fluid release led to fracturing and brecciation, and the formation of breccia pipes and clastic dikes (Svensen et al., 2010, 2020). Previous work on the contact areoles around sills in the Ecca Group indicated that the degassing and volatilization of shales could have released significant volatiles into the atmosphere, and due to the shale-rich nature of the Ecca Group, it is the most significant potential contributor of thermogenic gas from the Karoo basin (e.g., Svensen et al., 2007; Aarnes et al., 2010; Galerne and Hasenclever, 2019; Svensen et al., 2020).

3. Methods

Samples for geochronology were collected during fieldwork in 2008, targeting pegmatitic patches in dolerite sills in quarries and road cuts across the basin. Additional coarse sill samples were collected from the QU1/65 borehole at the core library of the Council for Geoscience in Pretoria, South Africa. The QU1/65 borehole contains ten sills (representing 22% of the drilled strata), including nine emplaced within the Ecca Group (Svensen et al., 2014). All samples were crushed in a tungsten mill, sieved to less than 300 μm, and then concentrated to heavy minerals using a Wilfley table, Frantz magnetic separation and heavy liquids. Backscatter electron (BSE) and cathodoluminescence (CL) images were acquired using a JOEL JSM7001F Thermal Field Emission SEM (Schottky electron gun) at the University of Geneva. Mineral inclusions in zircon were identified using energy dispersive spectroscopy (EDS). These techniques were used to characterize the internal textures and the inclusions within the crystals, in order to understand potential growth processes.

Baddeleyite and zircon were prepared and analyzed for ID-TIMS U-Pb geochronology using the methods detailed in Appendix Text 1. Reported $^{206}Pb/^{238}U$ dates were corrected for initial ^{230}Th disequilibrium. Earthtime 100 Ma standard solution analyzed during the period of these analyses yielded a $^{206}Pb/^{238}U$ date of 100.176 ± 0.006 Ma (MSWD = 2; n = 22), within uncertainty of the recently reported inter-laboratory calibrated value of 100.173 ± 0.003 Ma for this solution (Schaltegger et al., 2021).

Detailed methods for Hf isotope measurements can be found in Appendix Text 2. Data reduction to obtain the $^{176}Hf/^{177}Hf$ ratio included on peak zero baseline correction, correction for mass bias induced by the mass spectrometer measurement, correction

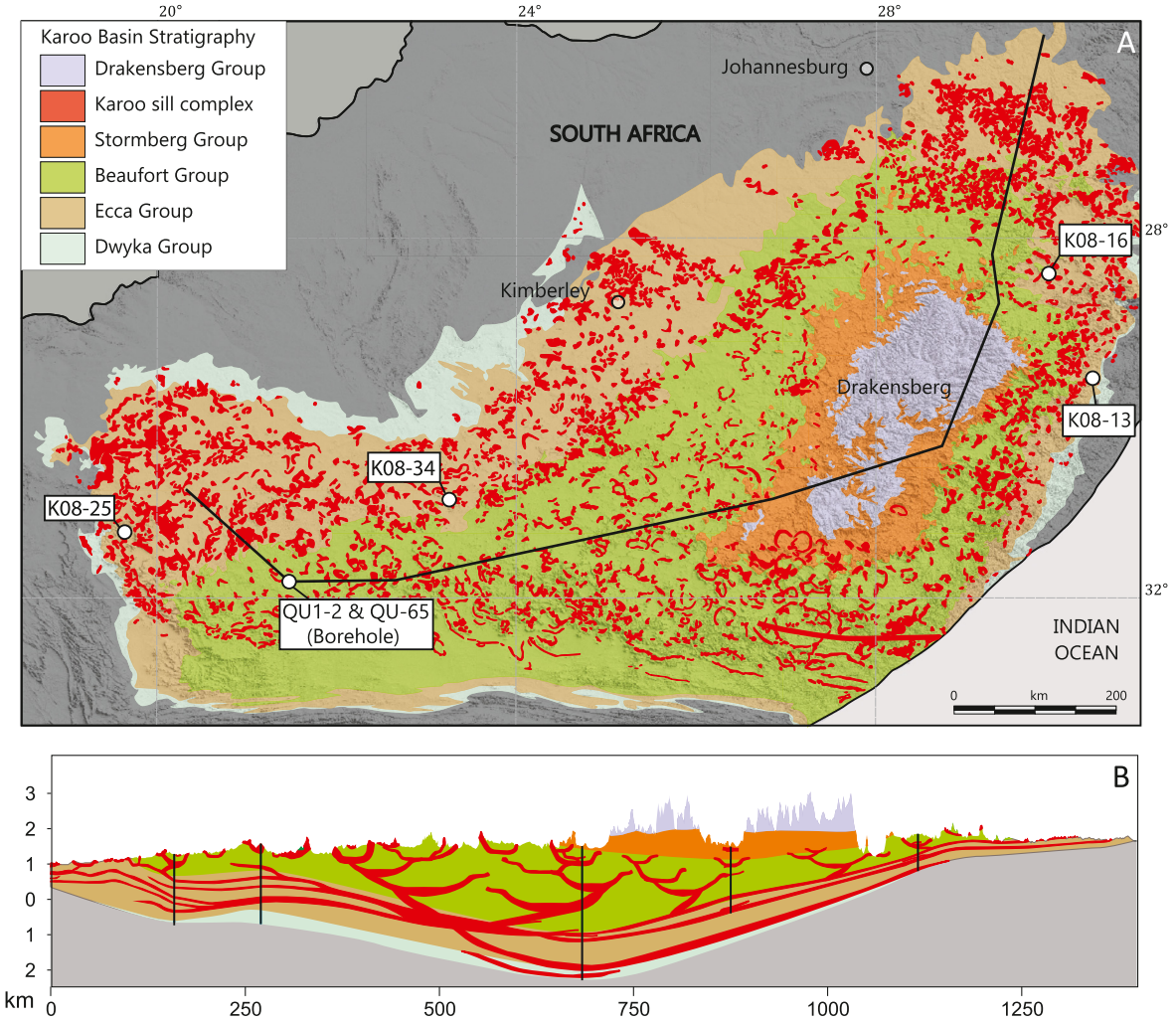

Fig. 1. Geological map (A) and cross section (B) of the Karoo Basin, showing the sampling sites of sills in the Ecca group dated in this study. The line defined by A-A′ on the map represents the cross section shown in Fig. 1B. Map and cross section modified from Svensen et al. (2012). (For interpretation of the colors in the figure(s), the reader is referred to the web version of this article.)

of isobaric interferences of ^{176}Lu and ^{176}Yb on ^{176}Hf and an offset correction by adjusting the ^{176}Hf/^{177}Hf ratio of the sample for the observed difference between the measured (0.272167 ± 0.000019, n = 46) and preferred value of the JMC475 Hf standard (i.e. 0.282160; Nowell et al., 1998). Due to the low analyte mass of zircon following chemical abrasion, Hf signal intensity was commonly low, and therefore the uncertainty on individual analyses varies, with some low abundance samples yielding higher uncertainties. The average ^{176}Hf/^{177}Hf ratio of all measured Plešovice solutions during the period of sample analyses is 0.28248 ± 0.00002 (n = 22), which translates to a εHf value of −3.2 ± 0.8 (2SD) at an age of 336.79 Ma (Widmann et al., 2019). This is identical within error to the proposed value in literature of εHf = −3.5 ± 1.5 (Sláma et al., 2008). All εHf uncertainties discussed in the text and shown in figures are reported at the 2σ uncertainty level.

4. Results

4.1. Zircon from pegmatites in the Ecca Group

Samples were collected from pegmatitic pods within dolerite sills throughout the Ecca Group, including several samples previously dated by Svensen et al. (2012) (QU1-2, K08-13, K08-16, K08-34), based on past success in isolating zircons from these textures. Previous studies were able to isolate zircon from coarse-grained portions of sills in other stratigraphic groups from the Karoo Basin (e.g., Svensen et al., 2007, 2012; Burgess et al., 2015; Greber et al., 2020), but this was not possible for the Ecca Group sills. The challenge of finding zircons in dolerite is illustrated by our new work: only two out of the eighteen bulk dolerite samples newly processed for this study yielded zircon or baddeleyite. The dolerites were sampled in a targeted field campaign where only pegmatoids were collected. Zircon from the pegmatitic pods within the Ecca formation is more abundant, but is of poor quality. The grains commonly display fractures, inclusions and altered domains (Fig. 2). Representative grains imaged using SEM commonly host inclusions, including apatite, amphibole, and feldspar. Both samples K08-13 and K08-16 had zircon with abundant fluid inclusions. Faint zonation was observed in the BSE imagery. In CL-imagery, grains did not yield strong cathodoluminescence, and therefore only minor zoning was observed and no obvious cores were observed in the grains (Fig. 2). Suppressed cathodoluminescence in zircon is commonly associated with decay-damage related metamictisation.

4.2. ID-CA-TIMS U-Pb geochronology

Chemical abrasion on zircon is commonly done as a partial dissolution of thermally annealed grains for 12 hours at 210 °C, to remove defect domains of zircons which have undergone Pb-loss

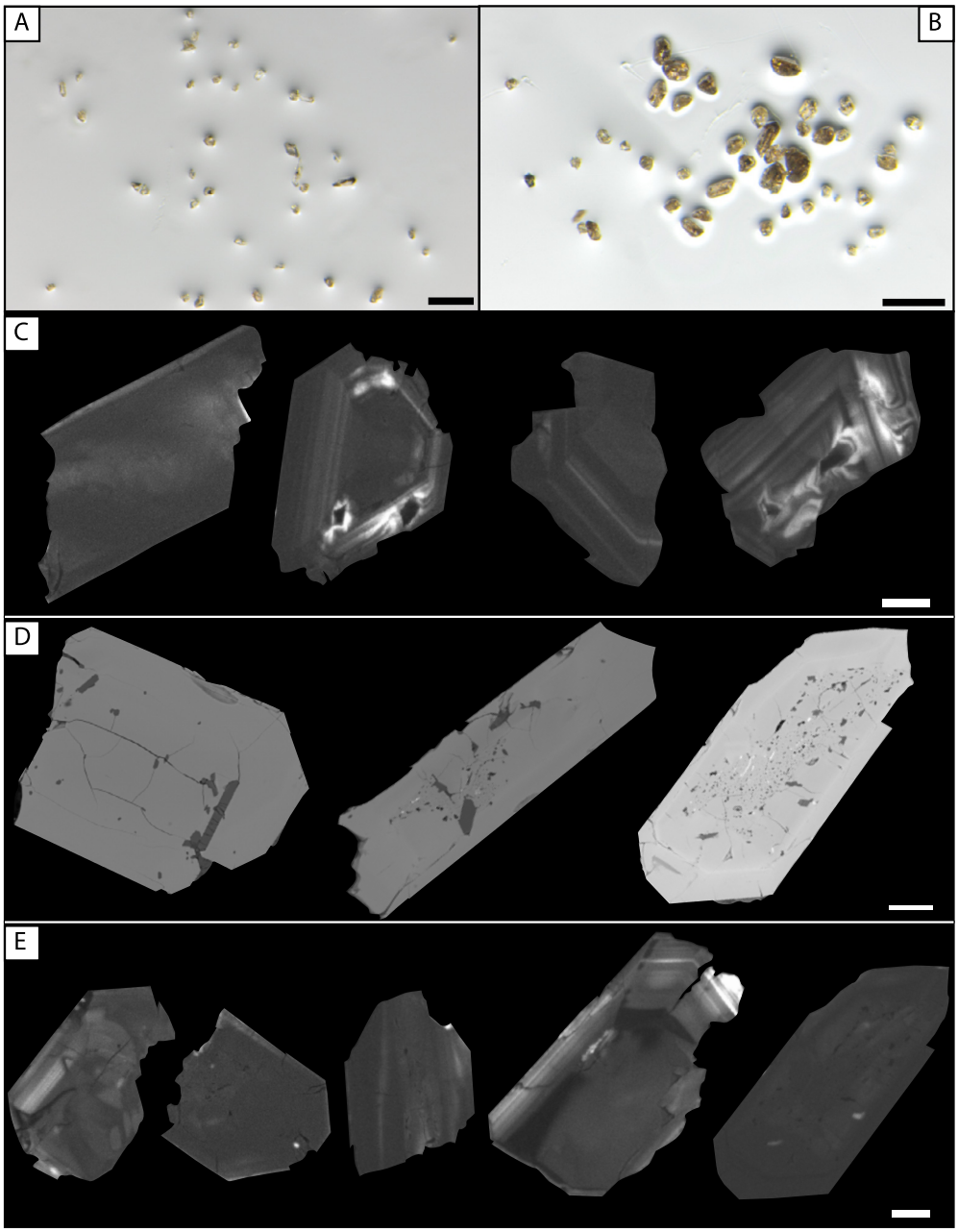

Fig. 2. Representative zircon imagery from samples QU1-2 (A, C) and K08-13 (B, D, E), showing optical (A & B), secondary electron microscope (SEM; D) and cathodoluminescence (CL; C & E) textures for zircon from pegmatitic pods in dolerite sills emplaced in the Ecca Group of the Karoo Basin. Scale bars are 200 µm for Fig. 2A & B, 20 µm for D, E and F. Only few zircon crystals imaged in this study yield significant cathodoluminescence, which is common among metamict zircon. Zircon from samples K08-13 and K08-16 commonly host abundant fluid inclusions within the grains, which do not appear to be associated with fractures or post-crystallization alteration (D).

or contain inclusions (e.g., Widmann et al., 2019). Unfortunately, the zircons in this study rapidly dissolved, with many zircons undergoing complete dissolution in less than 6 hours, pointing to elevated U concentrations and a metamict state of the crystal lattice. Therefore, the data presented in this study are from grains that have undergone only 6 hours of chemical abrasion at 210 °C. This duration was chosen as a compromise to at least partly mitigate Pb-loss, while retaining enough residual zircon material to date.

Individual $^{206}Pb/^{238}U$ dates of each sample span a considerable range and include normally discordant ages both older and younger than the main clusters of ages, as well as significant scatter among concordant dates (Fig. 3; Table A.1). A borehole sample of the 158 m thick sill intruding along the Ecca-Beaufort contact (QU1-2) represents the structurally highest intrusion in the Ecca group and was sampled at a core depth of 275.5 m. Zircon from this sample split into two populations, with two grains dated at approximately 184 Ma, and the remaining five grains overlapping at approximately 183.2 Ma. Sample QU-65 from a sill in the same borehole, 1,398.4 m from the surface, also yielded zircon. Fifteen grains were concordant with a large age range ($\Delta t = 13.54$ Ma), from 183.06 to 196.60 Ma and one normally discordant grain at 194.05 Ma, with a cluster of grains at approximately 183.2 Ma. A final drill core sample (674-423) yielded few zircon grains, the only grain surviving chemical abrasion yielded a normally discordant $^{207}Pb/^{206}Pb$ age of 2679.1 Ma. A sample of the upper Ecca Group (K08-16) from the eastern margin of the Karoo Basin (Fig. 1) yields a large range of single zircon dates ($\Delta t = 3.15$ Ma), without

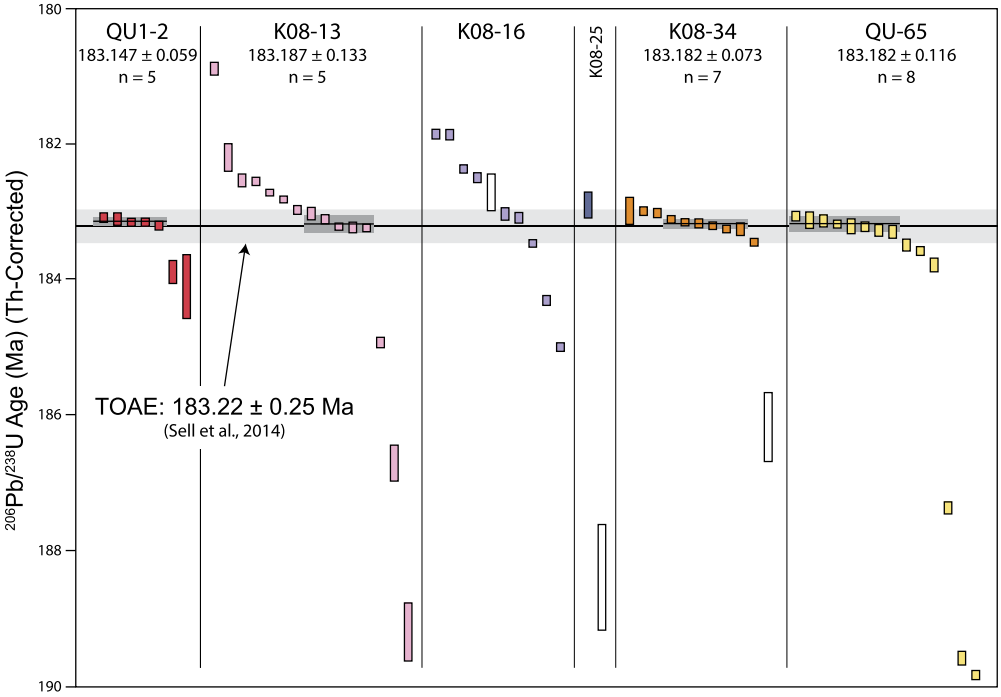

Fig. 3. $^{206}Pb/^{238}U$ ages for individual zircons for samples from sills in the Ecca group of the Karoo Basin. Vertical bar height is 2σ analytical uncertainties. As a result of these complicated age spectra of individual analyses, no sample age is estimated for the several samples (K08-16 and K08-25). For the remaining samples, we present the weighted mean and uncertainty for the plateau of grains which overlap within uncertainty (horizontal bars and boxes, respectively). Unfilled boxes represent normally discordant zircon analyses, all other analyses are concordant. The gray line across the entire figure represents the age of the TOAE (Sell et al., 2014). The weighted means for all interpreted samples overlap in age with the TOAE. See text for discussion.

a significant cluster of ages. Data from K08-13, a sill from the base of the Ecca Group at the eastern margin of the basin, have a large spread in dates (Δt =8.32 Ma), with a cluster of five grains at approximately 183.2 Ma. A pegmatitic enclave from the upper Ecca Group (K08-34) was sampled in the northwestern portion of the Karoo Basin. Zircon crystals from this sample had a more limited age range in concordant analyses (Δt = 458 ka) centered around 183.2 Ma, with one older, normally discordant grain. Finally, the farthest western sample in this study, K08-25, yielded few grains and most dissolved completely during a 6-hour chemical abrasion. The two grains which survived chemical abrasion yielded normally discordant ages of 188.4 and 182.9 Ma.

In two samples, we obtained additional $^{206}Pb/^{238}U$ dates from baddeleyite in addition to zircon (K08-16 and QU1-2; Fig. 4; Table A.2). Four grains from K08-16 are concordant and have ages ranging between 182.64 to 181.68 Ma, with one normally discordant younger grain at 122.7 Ma (not shown in Fig. 4). Sample QU1-2 yielded six concordant baddeleyite grains, with ages ranging from 182.95 to 180.72 Ma, all younger than zircon.

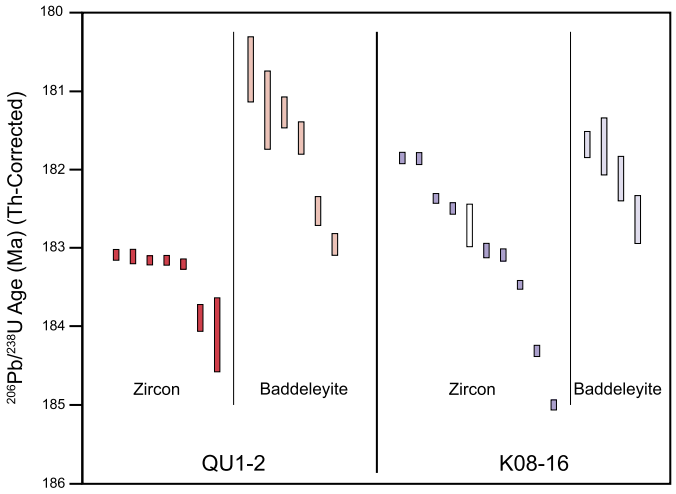

Fig. 4. Comparison of $^{206}Pb/^{238}U$ age spectra from zircon and baddeleyite grains from samples QU1-2 and K08-16 from pegmatitic pods in dolerite sills within the Ecca group, highlighting that unmitigated Pb-loss in baddeleyite likely yields inaccurate, younger ages within these samples. Analyses with white boxes are normally discordant.

4.3. MC-ICPMS zircon Hf isotope geochemistry

There is significant variability between the Hf isotope composition of zircon from different samples, and in several cases, between grains of the same sample (Fig. 5; Table A.3). Analyses from samples K08-13 and K08-16 span a considerable range, with εHf ranging from approximately −15 to −25, with an outlier at 0, and the isotope composition does not correlate with $^{206}Pb/^{238}U$ age. Nine zircon analyses from sample K08-34 overlap at approximately εHf = 2, with one slightly more radiogenic outlier at 5.1 ± 2.7. Seven grains from sample QU1-2 overlap at approximately εHf = 1.7, with outliers at −2.8 and 6.1. Zircon from sample QU-65 have εHf compositions ranging from −6.0 to 5.7, and there is no trend between age and composition. There were no observed differences between the Hf compositions of baddeleyite and zircon grains analyzed from the same sample (K08-16 and QU1-2).

5. Discussion

A detailed reevaluation of zircon geochronology from dolerite sills emplaced in the Ecca Group yields new insight into the systematics of zircon crystallization in mafic sills of LIPs. Evaluation of the SEM imagery, U-Pb geochronology and Hf isotope geochemistry indicates that zircon within these mafic horizons is unlikely to have formed through a closed-system fractionation. Instead, based on zircon geochemistry and geochronology we suggest it is more

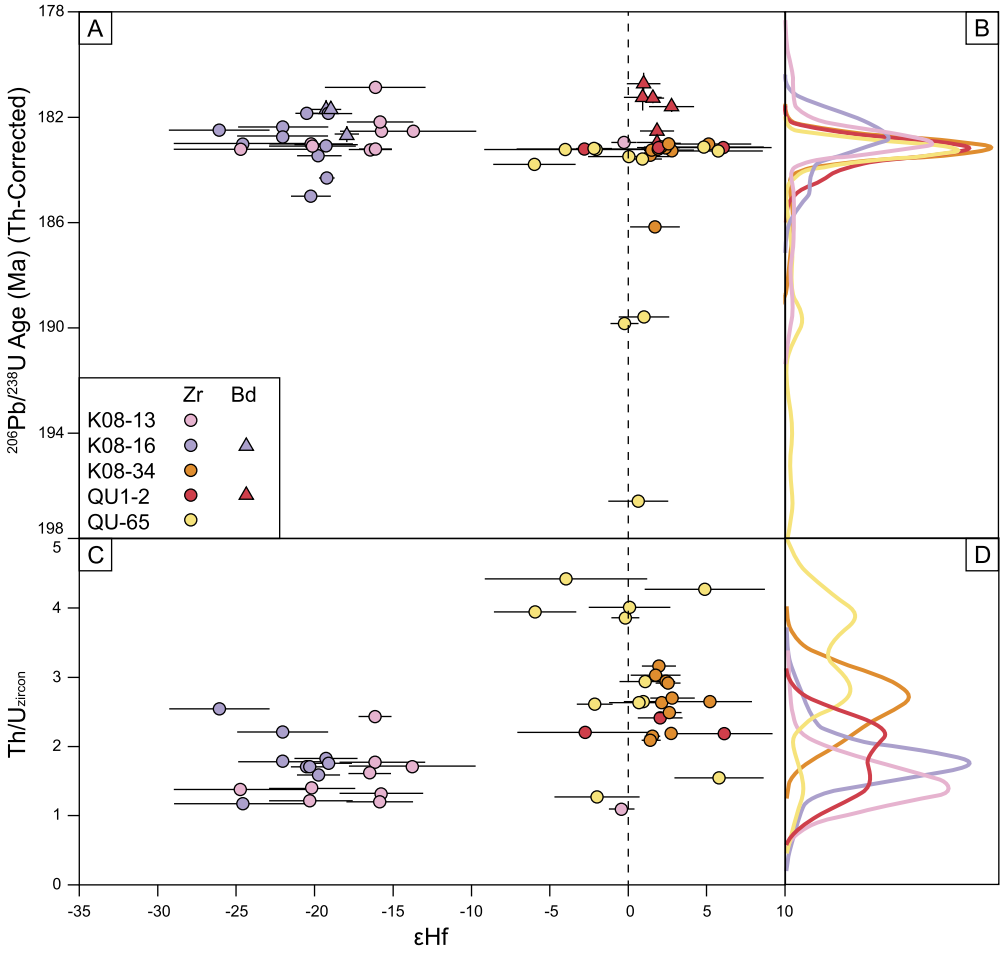

Fig. 5. Hf isotope composition of baddeleyite and zircon from Karoo LIP dolerite sills in the Ecca Group of the Karoo basin, compared to (A) $^{206}Pb/^{238}U$ age and (B) Th/U ratio. Insets B and D show kernel density estimates for the distribution of ages and Th/U compositions respectively, and include all samples analyzed in this study, including some not analyzed for Hf composition. See text for further discussion.

likely that the assimilation of clastic sedimentary wall rocks and the subsequent volatile generation and partial melting were necessary to form the pegmatitic segregations, which allow for the potential for high precision geochronology of this mafic LIP. Based on this scenario, we can interpret our highly complex data set in terms of emplacement and solidification of the sills within the Ecca Group. Our results yield overlapping ages between 183.147 ± 0.059 Ma and 183.187 ± 0.133 Ma for the sills in the Ecca Group, calculated using the grains interpreted to accurately reflect crystallization of the sills (Fig. 3). Our interpreted emplacement ages of these sills are identical within uncertainty to the age of the TOAE, based on previous geochronology of ash beds bracketing the carbon isotope excursion (183.22 ± 0.25 Ma; Sell et al., 2014), which supports that sill emplacement and subsequent degassing of sedimentary rocks presents a causal link to the global carbon cycle perturbation and climate change. Overall, these results suggest that future geochronological research on LIPs requires careful investigation and interpretation, as the combination of Pb loss from high-uranium zircon together with inheritance of old Pb components from detrital zircon in the clastic sediments can yield geologically inaccurate ages for emplacement.

5.1. How did zircon crystallize in dolerite sills in the Karoo Basin?

Dolerite sills within the Karoo Basin solidified within 100-1,000 years following emplacement depending on sill thickness and emplacement depth (e.g., Svensen et al., 2012). Previous geochemical studies indicate that these melts should not have saturated antecrystic zircon prior to crystallization at the emplacement level (e.g., Borisova et al., 2020). Therefore, if zircon crystallized from an intercumulus residual melt during fractionation of the dolerite magma, the geochronological dispersion within the zircon data from these sills should be well below the analytical ability of temporal resolution for a lower Jurassic age (0.1-0.02% of a $^{206}Pb/^{238}U$ date, i.e. 180,000 to 36,000 years). Consequently, all analyzed grains from an individual sample should be coeval in age within analytical error. Such data sets have resulted from previous geochronology research on Karoo dolerite dikes and sills, either generated from lower precision measurements of zircon from pegmatitic pods, or from coarse-grained sills (e.g., Svensen et al., 2007, 2010; Sell et al., 2014; Burgess et al., 2015; Greber et al., 2020). In addition, if zircon were crystallizing from an in-situ magmatic segregation, there should be minimal heterogeneity in Hf isotope compositions. Previously published Hf isotope compositions of bulk-separated zircon and baddeleyite grains from coarse-grained sills have been fairly homogeneous, with CHUR-like values, consistent with a mantle-derived magma genesis (Greber et al., 2020).

This model of zircon crystallization does not fit the observations from the pegmatoids in this study. While new analyses of samples previously dated in Svensen et al. (2012) are within uncertainty of previous data, these new analyses have significantly decreased uncertainty, and it is not possible to consider these samples as yielding single, overlapping age populations (Fig. A.1). Therefore, it is highly likely that these grains reflect more complex crystallization processes than previously ascribed to zircon within Karoo dolerites. These processes must be able to account for the follow-

ing observations within this data set and past work on the Karoo dolerite pegmatite-hosted zircons: (1) the presence of inheritance within zircon age spectra; (2) heterogeneities within the Hf compositions of zircons found within a single hand sample (e.g., K08-13; Fig. 5); (3) nonradiogenic Hf compositions; and (4) extremely high [U] in zircon (up 22,000 ppm; Svensen et al., 2012).

In order to crystallize zircon in pegmatitic pods in fine-grained dolerite sills in the Karoo, we suggest that the pods formed as a result of localized assimilation of sedimentary wall rock, including the possibility that thermogenic volatiles extended the presence of melt by lowering the solidus. In this model, rapid dissolution of fragmented sedimentary wall rock introduces silica and xenocrystic zircon material into the crystallizing dolerite melt, fundamentally changing melt composition towards more silicic conditions, and inducing zircon saturation. This would lead to heterogeneous nucleation of newly crystallizing zircon and overgrowth on pre-existing xenocrysts; this process would not necessarily involve every zircon, and the ratio of xenocrystic vs. autocrystic material would be variable from grain to grain. While the mafic composition of the dolerites is undersaturated relative to crystallization of zircon and would dissolve zircon in the melt, it is unlikely there was complete dissolution of xenocrysts during the brief period of cooling before solidification. The process is best traced by the variation in εHf, with very non-radiogenic compositions present in ~183.15 zircons even without any visible inherited cores (Figs. 2, 5). This parallels a trend in Th/U in zircon, where samples with more radiogenic Hf compositions tend to have higher Th/U ratios (Fig. 5). Zircon crystals in evolved residual melts from the Central Atlantic Magmatic Province (CAMP) have elevated Th/U ratios due to subordinate earlier crystallization of Th-scavenging minerals (Schaltegger and Davies, 2017). From this we deduce that Karoo samples with higher εHf and Th/U crystallized from a less contaminated magma. In addition, the Karoo melt pods must have contained sediment-derived fluids, as indicated by the abundance of fluid inclusions in zircon (Fig. 2). We therefore conclude that contamination was a continual process during emplacement and sill solidification. This connection between contamination and the presence of zircon is further supported by geochemical studies of the Golden Valley sills, which show evidence of fractionation and melt evolution marked by increased Si and Zr concentrations, but do not host zircon (e.g., Neumann et al., 2011).

The addition of basin-derived fluids may have introduced additional U and caused the growth of zircon extremely rich in U, and the high U concentrations and U/Th in dolerites in the Karoo Basin have previously been interpreted as the result of contamination from stratiform uranium ore bodies (Neumann et al., 2011). This additional of U-rich fluids during zircon crystallization would explain the abundance of likely Pb-loss in zircon from samples K08-13 and K08-16, which crystallized in more contaminated dolerite melts based on εHf and Th/U compositions. These fluids would also have further contaminated the pods, but likely are not directly responsible for the nonradiogenic Hf compositions observed in those samples, due to the low abundance of Hf in hydrothermal fluids. Furthermore, in the presence of fluid-saturated conditions, pegmatitic crystallization can occur at orders of magnitudes higher than normal igneous crystallization (Phelps et al., 2020). This observation may help explain why zircons were capable of growing larger than 100 µm along the elongate axis in spite of the rapid solidification timeframes of these sills.

A similar model of zircon crystallization via contamination was recently proposed by Davies et al. (2021), where assimilation of wall rock shales is a crucial factor in the crystallization of zircon within sills of the Central Atlantic Magmatic Province (CAMP). However, this work insinuated that the isolated melt pods were largely a function of solidification of an evolved liquid from fractionation of basaltic melt, which also incorporated assimilation of wall rock disseminated throughout the melt. While assimilation of high silica, upper crustal material can certainly help facilitate zircon saturation, the paucity of zircon in the surrounding fine-grained dolerite and considerable compositional variability among individual pegmatitic-pod zircon crystals suggests that assimilation was a far more localized process in the Karoo case, or that the pods represent a localized, greater contribution from assimilation of wall rock. Furthermore, the short timescales of sill solidification suggest that melting and complete mixing of molten wall rock material with mafic magma is unlikely prior to final solidification of these sills at the emplacement level, especially as assimilation thermodynamically induces crystallization of the host magma (Glazner, 2007). Therefore, it is hard to support widespread, well-mixed contamination of LIP intrusions at the emplacement level with the data presented in this study.

5.2. Interpretation of U-Pb zircon & baddeleyite ages

As a direct consequence of the processes described above, U-Pb results presented here are quite complicated, with many samples demonstrating age spectra that are unlikely to be the result of crystallization from a rapidly cooling and solidifying magma. While some of these age spectra show significant dispersion of the $^{206}Pb/^{238}U$ dates, several populations include statistically relevant sub-populations ("clusters"), which we argue are equivalent of the high-precision crystallization age for the respective samples. The presence of inheritance is quite clear in many of the samples, given how anomalously older ages are commonly normally discordant, and best highlighted by the 2.679 Ga $^{207}Pb/^{206}Pb$ age of a zircon sampled from sample 674-423. Therefore, older zircon dates are likely a function of the volumetric mixture of new autocrystic zircon growth and inherited xenocrystic components from the partial melting of sedimentary material. The degree of discordance would then depend on the age offset relative to the precision of the individual data point.

It is rather common to dismiss the impact of Pb loss on zircon age spectra, because the thermal annealing–chemical abrasion technique employed in most labs (as well as in this study) has proven highly effective at removing volumes of zircon damaged by radioactive decay (Schaltegger and Davies, 2017; Widmann et al., 2019). The analytical procedures in Svensen et al. (2012) did not utilize chemical abrasion as a means for removing zircon domains with damaged lattice, but instead used mechanical air abrasion. The analyzed material consisted of coherent zircon grains that could be weighed, and therefore the authors were able to indicate the concentrations of U and Th of dated zircon. Values up to 20,000 ppm U indicate that many of the grains have undergone significant α-decay damage, leading to aperiodic crystal regions with multiple overlaps of displacement cascades accumulating damage beyond the second percolation threshold (Murakami et al., 1991) that acted as fast pathways for Pb-loss (Fig. A.2; e.g., Pidgeon, 2014). This interpretation is in agreement with the suppression of cathodoluminescence, as well as the rapid dissolution of these zircon during experimental chemical abrasion (e.g., Krogh and Davis, 1975). Given this situation, chemical abrasion at 210 °C for six hours may not be totally effective as pretreatment, and therefore we interpret that the young tails on some of the zircon age spectra are the result of unmitigated Pb-loss. This interpretation is furthered by the presence of a 182.71 Ma normally discordant zircon analysis from K08-16, indicative of open system U-Pb behavior. This open system behavior is more apparent in this dataset rather than past work due to increased precision (Fig. A.1). Furthermore, for previous analyses of zircon from the Karoo, grains with lower Th/U compositions are more likely to have significant α-dose values, and therefore heavy contamination during crystal-

lization may coincide with the growth of high-U zircon unfavorable for total mitigation of Pb-loss (Fig. A.3).

While several samples in this study did not produce enough zircon and/or have coherent age plateaus (K08-16, K08-25, 674-423) and therefore fail to indicate a reliable age, we suggest that other samples reliably date crystallization and solidification of the sills (QU1-2, QU-65, K08-13, K08-34). Taking a weighted mean of these plateaus yields unacceptably high MSWD values, up to 5.9, indicative that the observed plateaus do not represent a single age population. Calculating a weighted mean value using a subset of each plateau can yield acceptable MSWD values, but doing so could bias the age towards inaccuracy due to the inherent complexities of these zircon. As a result, we instead calculate weighted mean ages using the entire overlapping plateau, and then use a conservative, larger estimate of uncertainty using half of the difference between the oldest and youngest grains in the plateau in order to best maintain accurate age calculation (Fig. 3). Using the criteria outlined above and this method of uncertainty calculation, we interpret that QU1-2 crystallized at 183.147 ± 0.059/0.086/0.229 Ma (n = 5), QU-65 at 183.182 ± 0.029/0.056/0.20 (n = 8), K08-13 at 183.187 ± 0.133/0.159/0.313 Ma (n = 5), and K08-34 at 183.182 ± 0.073/0.103/0.249 Ma (n = 6; all errors at 2σ; Fig. 3). Given the uncertainty of these analyses and the geographic spread of the samples, these data indicate that sill emplacement throughout the Ecca Group was synchronous at the ~100 ka level of precision. Thermal models indicate that individual sills cooled to solidus likely in significantly less than 10,000 years depending on the sill thicknesses (e.g., Svensen et al., 2012), and therefore sill emplacement may not have been perfectly coeval, however our new data place a far more precise temporal constraints on Ecca intrusions than previously available. The process of contact metamorphism and devolatilization will in any case start immediately following emplacement and proceed throughout the sill cooling period.

Recent work has begun to highlight that within the lifespan of LIPs, discrete periods may host far more rapid and voluminous intrusions and eruptions (e.g., Burgess et al., 2017; Schoene et al., 2019). Using these new zircon age interpretations, magma fluxes of intrusions into the Ecca Group range from 0.63 km^3/a to an instantaneous magma emplacement of 160,000 km^3, based on the uncertainty of these zircon age interpretations and previously established volumetric estimates for sills in the Ecca Group (Svensen et al., 2012). While comparable high-precision geochronology for the remainder of the intrusions throughout the basin is not currently available, the average magma flux for LIP intrusions in the Karoo Basin was previously estimated at 0.78 km^3/a (Svensen et al., 2012), and therefore sills in the Ecca Group may reflect a period of increased magma flux during the injection of the sub-volcanic component of the LIP.

Finally, the baddeleyite dated in this study does not yield coherent age spectra. We interpret these dates to represent variable degrees of Pb-loss, as mitigation via chemical abrasion does not work on baddeleyite (Rioux et al., 2010). While baddeleyite may be an active recorder of magmatic processes, these results suggest that further work may be required to obtain accurate dates from this mineral.

5.3. Implications for the contamination of Large Igneous Province intrusions

The effects of lower crustal assimilation on the geochemistry of asthenosphere-derived magmas in LIPs are well documented (e.g., Luttinen, 2018), and recent work has emphasized the potential effects of upper crustal assimilation in intrusions (e.g., Heimdal et al., 2019; Davies et al., 2021). However, the data from pegmatitic pods within dolerites in the Ecca Group indicates that the contamination and assimilation of crustal material into the mafic melts may locally produce unique geochemical and geochronological conditions. This contamination is variable and local, and likely requires specific emplacement processes to facilitate contamination, as the more fractionated sills elsewhere in the Karoo Basin do not necessarily form these pegmatitic pods (e.g., Neumann et al., 2011).

Zircon ID-TIMS U-Pb geochronology has been key in understanding the construction of silicic batholiths and eruptions because of its high precision and accuracy (e.g., Gaynor et al., 2019; Szymanowski et al., 2019), and therefore has been a highly pursued technique in LIP systems as well. In several cases, zircons from pegmatitic pods have yielded uniform age distributions, with this zircon interpreted as crystallized via advanced magma fractionation (e.g., Burgess et al., 2015). However, new data from this study and several recent studies on the CAMP and the Deccan Traps suggest that zircon within LIPs may crystallize due to magmatic contamination, enabling the ability to generate U-Pb zircon geochronology on these magmas. Unfortunately, this style of crystallization may also initially limit zircon's accuracy as an absolute geochronometer of magma crystallization without additional context. Recent work on CAMP sills in Brazil indicates that upper crustal assimilation, particularly of shales, helped drive crystallization of zircon within the mafic magmas, due to increased silica and water concentrations in the crystallizing melts. Those samples commonly yielded protracted age spectra beyond their expected cooling history (Davies et al., 2021). Both the Deccan Traps and Columbia River basalt flows rarely contain zircon, but a reliable, high-precision age models have been established almost entirely from zircon grains from oxidized volcaniclastic material and felsic ash beds interbedded between basalt flows (Kasbohm and Schoene, 2018; Schoene et al., 2019). These uncontaminated basalt flows may not have been capable of reaching zircon saturation, but alkalic intrusions temporally associated with the Deccan Traps do include zircon in many cases. Among those samples, many yielded protracted U-Pb age spectra and significantly non-radiogenic Hf compositions, indicative that zircon specifically recorded contamination (Basu et al., 2020). These datasets from the CAMP and Deccan Traps LIPs are similar to the data from the Karoo, wherein the basaltic lava stacks are largely devoid of zircon, only some coarse-grained sills and pegmatitic pods contain zircon, and zircon-bearing pegmatitic pods may be the result of magma contamination. Further work is needed to better understand the scale and modalities of contamination in LIP magmas, and how this process may be recorded by U-Pb geochronology.

5.4. Was the emplacement of sills in the Ecca Group correlative with the Toarcian Oceanic Anoxic Event?

Based on the four samples which yielded high-precision data corresponding to an emplacement age, basin-scale emplacement of sills within the Ecca Group occurred over a time period ranging between instantaneous intrusion to over 254 ka, based on the minimum and maximum age ranges possible from the uncertainties of the interpreted ages. These samples are hundreds of km from each other and are from different structural levels within the stratigraphy; therefore, our age model likely reflects the full emplacement of the 160,000 km^3 sill complex within the Ecca Group. Based on previous estimates of thermogenic CO_2 degassing from the Ecca Group (e.g., Svensen et al., 2007; Aarnes et al., 2010; Galerne and Hasenclever, 2019; Svensen et al., 2020; Heimdal et al., 2021), degassing was as low as 0.028 Gt CO_2/a over a period of 254 ka, or as fast as the instantaneous release of >50,000 Gt of CO_2. This amount of thermogenic degassing represents a plausible source for the observed negative carbon isotope excursions associated with the TOAE (Heimdal et al., 2021). These values do not account for the mantle-derived CO_2 inputs from magma ascent and sill crystallization, which have been shown to contribute large vol-

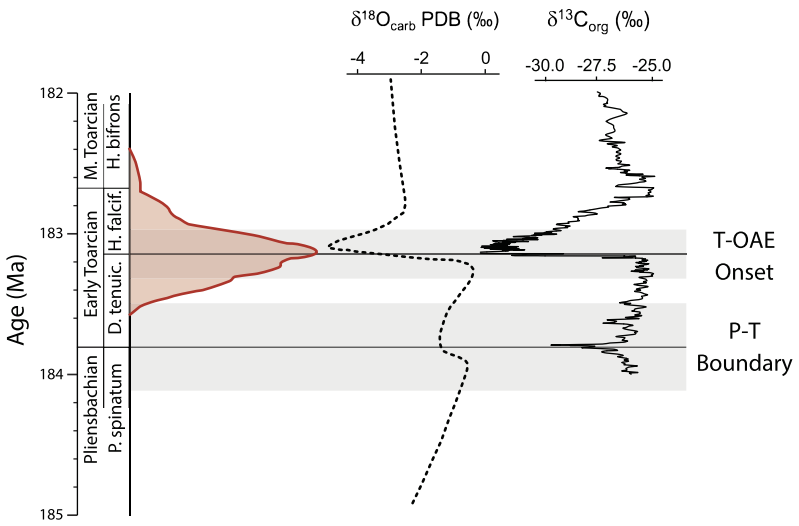

Fig. 6. Correlation of environmental proxies with a kernel density estimate of high-precision U-Pb ages from Karoo basin intrusions, highlighting the coeval timing of the onset of the Toarcian oceanic anoxic event (T-OAE), and the diachronous timing of the Pliensbachian-Toarcian boundary (P-T) with Karoo Basin magmatism. Oxygen isotope curve is an estimated average value from Korte et al. (2015), and the carbon isotope curve is from Ruebsam et al. (2019). Geochronology of the Karoo LIP from Sell et al. (2014), Burgess et al. (2015), Corfu et al. (2016), Greber et al. (2020) and this study. Ammonite zones are from Guex et al. (2012). Modified from Greber et al. (2020).

umes to the atmosphere in the case of the CAMP (Capriolo et al., 2020). Therefore, emplacement in the Ecca Group between 183.147 ± 0.059 Ma and 183.187 ± 0.133 Ma would lead to a geologically rapid, voluminous volatile generation, which is required to explain global environmental change and its proxy record, including the TOAE (Svensen et al., 2007; Heimdal et al., 2021).

A correlative, and potentially causative relationship between intrusive magmatism within the Karoo Basin and the TOAE has been long examined, especially in the context of a growing geochronologic database (e.g., Svensen et al., 2007, 2012; Sell et al., 2014; Burgess et al., 2015; Greber et al., 2020; Kasbohm et al., 2021). The early Jurassic is characterized by a series of environmental and biotic overturning events that most commonly are traced by mostly negative excursions of stable carbon and oxygen isotopes (Fig. 6) indicating thermal optima, partial oceanic anoxia and changes in the global biomass. These peaks coincide with biotic events of extinction and radiation on species and family levels (e.g., Danise et al., 2015) pointing to a driver for environmental change of global impact. The most prominent ones are the "late Pliensbachian event" (e.g., Korte and Hesselbo, 2011) which occurred before 184.02 ± 0.05 Ma (De Lena et al., 2019); at the Pliensbachian/Toarcian boundary at 183.8 ± 0.4 Ma (e.g., Ruhl et al., 2016; Rita et al., 2019) and in the early Toarcian at the base of the Falciferum ammonite zone, the TOAE dated at 183.22 ± 0.25 (e.g., Sell et al., 2014). Our new ages of 183.147 ± 0.059 Ma to 183.187 ± 0.133 Ma for the sill intrusion emplaced in the Ecca Group further strengthens the temporal coincidence with the TOAE and strengthens an argument for causality between LIP emplacement, and global environmental and biotic disturbance (Fig. 6).

6. Conclusions

New geochronology and isotope data from zircon and baddeleyite from pegmatitic pods within dolerite sills of the Karoo LIP emplaced in the Ecca Group indicate that they crystallized in regions of localized assimilation of clastic wall rock between 183.147 ± 0.059 Ma and 183.187 ± 0.133 Ma. This melt contamination enabled the crystallization of uraniferous accessory phases that are essential for high-precision geochronology; however, the composition and crystallization history of these crystals complicated the age spectra. Interpreting the age spectra of individual samples based on overlapping clusters of dates yields coeval, high-precision ages for sills in the Ecca Group throughout the Karoo Basin. These sills were therefore emplaced during a period of particularly high magma flux of Karoo LIP intrusive magmatism, relative to previous estimates. This sudden influx of magmas released a large volume of thermogenic gas from the basin, and due to the coeval timing of these intrusions and the TOAE, we suggest these sills were the trigger for this period of global climate change.

CRediT authorship contribution statement

Sean P. Gaynor: Formal analysis, Investigation, Writing – original draft, Writing – review & editing. **Henrik H. Svensen:** Resources, Writing – review & editing. **Stéphane Polteau:** Resources, Writing – review & editing. **Urs Schaltegger:** Funding acquisition, Writing – review & editing.

Declaration of competing interest

The authors declare that they have no known competing financial interests or personal relationships that could have appeared to influence the work reported in this paper.

Acknowledgements

This research was supported by the Swiss National Science Foundation project No. 200020_182007 to U.S. We acknowledge support to H.S. from the Research Council of Norway to CEED through its Centres of Excellence funding scheme, project 223272. Hafnium isotope measurements benefited from support from Nicolas Greber and Massimo Chiaradia, SEM imagery was supported by Ariadni Georgatou, and mineral separation work was supported by Mélissa Ruiz. Thanks to Editor Chiara Maria Petrone for the handling of the manuscript, and to Jennifer Kasbohm and Michael Eddy for thorough, constructive reviews of this manuscript. This manuscript also benefited from an early informal review from Sara Callegaro.

Appendix A. Supplementary material

Supplementary material related to this article can be found online at https://doi.org/10.1016/j.epsl.2022.117371.

References

Aarnes, I., Svensen, H.H., Connolly, J.A.D., Podladchikov, Y.Y., 2010. How contact metamorphism can trigger global climate changes: modeling gas generation around igneous sills in sedimentary basins. Geochim. Cosmochim. Acta 74, 7,179–7,195.

Basu, A.R., Chakrabarty, P., Szymanowski, D., Ibañez-Mejia, M., Schoene, B., Ghosh, N., Georg, R.B., 2020. Widespread silicic and alkaline magmatism synchronous with the Deccan Traps flood basalts, India. Earth Planet. Sci. Lett. 552, 10.

Bond, D.P.G., Wignall, P.B., 2014. Large igneous provinces and mass extinctions: an update. In: Keller, G., Kerr, A.C. (Eds.), Volcanism, Impacts and Mass Extinctions: Causes and Effects. In: Geological Society of America Special Papers, vol. 5050.

Borisova, A.Y., Bindeman, I., Toplis, M.J., Zagrtdenov, N.R., Guignard, J., Safonov, O.G., Bychkov, A.Y., Shcheka, S., Melnik, O.E., Marchelli, M., Fehrenbch, J., 2020. Zircon survival in shallow asthenosphere and deep lithosphere. Am. Mineral. 105, 1662–1671.

Bryan, S.E., Ernst, R.E., 2008. Revised definition of Large Igneous Provinces (LIPs). Earth-Sci. Rev. 86, 175–202.

Burgess, S.D., Bowring, S.A., Fleming, T.H., Elliot, D.H., 2015. High-precision geochronology links the Ferrar large igneous province with early-Jurassic ocean anoxia and biotic crisis. Earth Planet. Sci. Lett. 415, 90–99.

Burgess, S.D., Muirhead, J.D., Bowring, S.A., 2017. Initial pulse of Siberian Traps sills as the trigger of the end-Permian mass extinction. Nat. Commun. 8, 6.

Capriolo, M., Marzoli, A., Aradi, L.E., Callegaro, S., Dal Corso, J., Newton, R.J., Mills, B.J.W., Wignall, P.B., Bartoli, O., Baker, D.R., Youbi, N., Remusat, L., Spiess, R., Szabó, C., 2020. Deep CO_2 in the end-Triassic Central Atlantic Magmatic Province. Nat. Commun. 11.

Corfu, F., Svensen, H., Mazzini, A., 2016. Comment to paper: Evaluating the temporal link between the Karoo LIP and climatic-biologic events of the Toarcian stage with high-precision U-Pb geochronology by Bryan Sell, Maria Otcharova, Jean Guex, Annachiara Bartolini, Fred Jourdan, Jourge E. Spangenberg, Jean-Claude Vincente, Urs Scaltegger in *Earth and Planetary Science Letters*. Earth Planet. Sci. Lett. 434, 349–352.

Danise, S., Twitchett, R.J., Little, C.T.S., 2015. Environmental controls on Jurassic marine ecosystems during global warming. Geology 34, 263–266.

Davies, J.H.F.L., Marzoli, A., Bertrand, H., Youbi, N., Ernesto, M., Greber, N.D., Ackerson, M., Simpson, G., Bouvier, A.S., Baumgartner, L., Pettke, T., Farina, F., Ahrenstedt, H.V., Schaltegger, U., 2021. Zircon petrochronology in large igneous provinces reveals upper crustal contamination processes: new U-Pb ages, Hf and O isotopes, and trace elements from the Central Atlantic magmatic province (CAMP). Contrib. Mineral. Petrol. 176, 24.

De Lena, L.F., Taylor, D., Guex, J., Bartolini, A., Adatte, T., van Acken, D., Spangenberg, J.E., Samankassou, E., Vennemann, T., Schaltegger, U., 2019. The driving mechanisms of the carbon cycle perturbations in the late Pliensbachian (Early Jurassic). Sci. Rep. 9.

Duncan, R.A., Hooper, P.R., Rehacek, J., Marsh, J.S., Duncan, A.R., 1997. The timing and duration of the Karoo igneous event, southern Gondwana. J. Geophys. Res. 102, 18,127–18,138.

Galerne, C.Y., Hasenclever, J., 2019. Distinct degassing pulses during magma invasion in the stratified Karoo Basin - new insights from hydrothermal fluid flow modeling. Geochem. Geophys. Geosyst. 20, 2,955–2,984.

Gaynor, S.P., Coleman, D.S., Rosera, J.M., Tappa, M.J., 2019. Geochronology of a Bouguer gravity low. J. Geophys. Res., Solid Earth 124, 2,457–2,468.

Glazner, A.G., 2007. Thermal limitations on incorporation of wall rock into magma. Geology 35, 319–322.

Greber, N.D., Davies, J.H.F.L., Gaynor, S.P., Schaltegger, U., Jourdan, F., Bertrand, H., 2020. New high precision U-Pb ages and Hf isotope data from the Karoo large igneous province; implications for pulsed magmatism and early Toarcian environmental perturbations. Results Geochem. 1.

Guex, J., Bartolini, A., Spangenberg, J., Vicente, J.C., Schaltegger, U., 2012. Ammonoid multi-extinction crises during the Late Pliensbachian-Toarcian and carbon cyce instabilities. Solid Earth Discuss. 4, 1205–1228.

Heimdal, T.H., Callegaro, S., Svensen, H.H., Jones, M.T., Pereira, E., Planke, S., 2019. Evidence for magma-evaporite interactions during the emplacement of the Central Atlantic Magmatic Province (CAMP) in Brazil. Earth Planet. Sci. Lett. 506, 476–492.

Heimdal, T.H., Goddéris, Y., Jones, M.T., Svensen, H.H., 2021. Assessing the importance of thermogenic degassing from the Karoo Large Igenous Province (LIP) in driving Toarcian carbon cycle perturbations. Nat. Commun. 12.

Jourdan, F., Féraud, G., Bertrand, H., Watkeys, M.K., Renne, P.R., 2008. The $^{40}Ar/^{39}Ar$ ages of the sill complex of the Karoo large igneous province: implications for the Pliensbachian-Toarcian climate change. Geochem. Geophys. Geosyst. 9, 20.

Kasbohm, J., Schoene, B., 2018. Rapid eruption of the Columbia River flood basalt and correlation with the mid-Miocene climate optimum. Sci. Adv. 4, 9.

Kasbohm, J., Schoene, B., Burgess, S., 2021. Radiometric constraints on the timing, tempo and effects of Large Igneous Province emplacement. In: Ernst, R.E., et al. (Eds.), Large Igneous Provinces: A Driver of Global Environmental and Biotic Changes. In: AGU Geophysical Monograph, vol. 255, pp. 25–80.

Korte, C., Hesselbo, S.P., Ullmann, C.V., Dietl, G., Ruhl, M., Schweigert, G., Thibault, N., 2015. Jurassic climate mode governed by ocean gateway. Nat. Commun. 6, 59.

Krogh, T.E., Davis, G.L., 1975. Alteration in zircons and differential dissolution of altered and metamict zircon. In: Carnegie Institute Washington Yearbook, vol. 74, pp. 619–623.

Luttinen, A.V., 2018. Bilateral geochemical asymmetry in the Karoo large igneous province. Sci. Rep. 8.

Murakami, T., Chakoumakos, B.C., Ewing, R.C., Lumpkin, G.R., Weber, W.J., 1991. Alpha-decay event damage in zircon. Am. Mineral. 76, 1,510–1,532.

Neumann, E-R., Svensen, H., Galerne, C., Planke, S., 2011. Multistage evolution of magmas in the Karoo Large Igneous Province. J. Petrol. 52, 959–984.

Nowell, G.M., Kempton, P.D., Noble, S.R., Fitton, J.G., Saunders, A.D., Mahoney, J.J., Taylor, R.N., 1998. High precision Hf isotope measurements of MORB and OIB by thermal ionisation mass spectrometry: insights into the depleted mantle. Chem. Geol. 149, 211–233.

Phelps, P.R., Lee, C.T.A., Morton, D.M., 2020. Episodes of fast crystal growth in pegmatites. Nat. Commun. 11.

Pidgeon, R.T., 2014. Zircon radiation damage ages. Chem. Geol. 367, 13–22.

Rioux, M., Bowring, S., Dudás, F., Hanson, R., 2010. Characterizing the U-Pb systematics of baddeleyite through chemical abrasion: application of multi-step digestion methods to baddeleyite geochronology. Contrib. Mineral. Petrol. 160, 777–801.

Rita, P., Nätscher, P., Duarte, L.V., Weis, R., De Baets, K., 2019. Mechanisms and drivers of belemnite body-size dynamics across the Pliensbachian-Toarcian crisis. R. Soc. Open Sci. 6.

Ruebsam, W., Mayer, B., Schwark, L., 2019. Cryosphere carbon dynamics control early Toarcian global warming and sea level evolution. Glob. Planet. Change 172, 440–453.

Ruhl, M., Hesselbo, S.P., Hinnov, L., Jenkyns, H.C., Xu, W., Riding, J.B., Storm, M., Minisini, D., Ullmann, C.V., Leng, M.J., 2016. Astronomical constraints on the duration of the Early Jurassic Pliensbachian Stage and global climatic fluctuations. Earth Planet. Sci. Lett. 455, 149–165.

Schaltegger, U., Davies, J.H.F.L., 2017. Petrochronology of zircon and baddeleyite in igneous rocks: reconstructing magmatic processes at high temporal resolution. Rev. Mineral. Geochem. 83, 297–328.

Schaltegger, U., Ovtcharova, M., Gaynor, S.P., Schoene, B., Wotzlaw, J., Davies, J.H.F.L., Farina, F., Greber, N., Szymanowskit, D., Chelle-Michou, C., 2021. Long-term repeatability and interlaboratory reproducibility of high-precision ID-TIMS U-Pb geochronology. J. Anal. At. Spectrom. 36, 1,466–1,477.

Schoene, B., Eddy, M.P., Samperton, K.M., Keller, B.C., Keller, G., Adatte, T., Khadri, S.F.R., 2019. U-Pb constraints on pulsed eruption of the Deccan Traps across the end-Cretaceous mass extinction. Science 363, 862–866.

Self, S., Schmidt, A., Mather, T.A., 2014. Emplacement characteristics, time scales, and volcanic gas release rates of continental flood basalt eruptions on Earth. Geol. Soc. Am. Spec. Pap. 505, 319–337.

Sell, B., Ovtcharova, M., Guex, J., Bartolini, A., Jourdan, F., Spangenberg, J.E., Vicente, J.C., Schaltegger, U., 2014. Evaluating the temporal link between the Karoo LIP and climatic-biologic events of the Toarcian Stage with high-precision U-Pb geochronology. Earth Planet. Sci. Lett. 408, 48–56.

Sláma, J., Košler, J., Condon, D.J., Crowley, J.L., Gerdes, A., Hanchar, J.M., Horstwood, M.S.A., Morris, G.A., Nasdala, L., Norberg, N., Schaltegger, U., Schoene, B., Tubrett, M.N., Whitehouse, M.J., 2008. Plešovice zircon — a new natural reference material for U–Pb and Hf isotopic microanalysis. Chem. Geol. 249, 1–35.

Svensen, H., Jamtveit, B., Planke, S., Chevallier, L., 2006. Structure and evolution of hydrothermal vent complexes in the Karoo Basin, South Africa. J. Geol. Soc. 163, 671–682.

Svensen, H., Planke, S., Chevallier, L., Malthe-Sorenssen, A., Corfu, F., Jamtveit, B., 2007. Hydrothermal venting of greenhouse gases triggering Early Jurassic global warming. Earth Planet. Sci. Lett. 256, 554–566.

Svensen, H., Aarnes, I., Podladchikov, Y.Y., Jettestuen, E., Harstad, C.H., Planke, S., 2010. Sandstone dikes in dolerite sills: evidence for high-pressure gradients and sediment mobilization during solidification of magmatic sheet intrusions in sedimentary basins. Geosphere 6, 211–224.

Svensen, H., Corfu, F., Polteau, S., Hammer, Ø, Planke, S., 2012. Rapid magma emplacement in the Karoo Large Igneous Province. Earth Planet. Sci. Lett. 325–326, 1–9.

Svensen, H.H., Polteau, S., Cawthorn, G., Planke, S., 2014. Sub-volcanic Intrusions in the Karoo Basin, South Africa. In: Breitkreuz, C., Rocchi, S. (Eds.), Physical Geology of Shallow Magmatic Systems. In: Advances in Volcanology (An Official Book Series of the International Association of Volcanology and Chemistry of the Earth's Interior). Springer, Cham.

Svensen, H.H., Hammer, Ø, Chevallier, L., Jerram, D.A., Silkoset, P., Polteau, S., Planke, S., 2020. Understanding thermogenic degassing in large igneous provinces: inferences from the geological and statistical characteristics of breccia pipes in the western parts of the Karoo Basin. In: Adatte, T., Bond, D.P.G., Keller, G. (Eds.), Mass Extinctions, Volcanism, and Impacts: New Developments. In: Geological Society of America Special Papers, vol. 544.

Szymanowski, D., Ellis, B.S., Wotzlaw, J.F., Bachmann, O., 2019. Maturation and rejuvenation of a silicic magma reservoir: high-resolution chronology of the Kneeling Nun Tuff. Earth Planet. Sci. Lett. 510, 103–115.

Widmann, P., Davies, J.H.F.L., Schaltegger, U., 2019. Calibrating chemical abrasion: its effects on zircon crystal structure, chemical composition and U-Pb age. Chem. Geol. 511, 1–10.